Role of Sn in the Amorphous-to-Crystalline Transition of TiO_2 Thin Films

Pritha Biswas[1], Tamara D. Koledin[2,3], Skylar N. Farmer[1], Melissa K. Santala,[2,3], and Janet Tate[1]

[1]Department of Physics, Oregon State University, Corvallis, Oregon 97331, USA

[2]Materials Science Program, Oregon State University, Corvallis, OR 97331, USA

[3]Department of Mechanical, Industrial, and Manufacturing Engineering, Oregon State University, Corvallis, OR 937331, USA

Abstract:

The amorphous-to-crystalline transition in TiO_2 films upon annealing in air yields different polymorphs depending on the oxygen partial pressure during the deposition of the amorphous precursor film. We further manipulate the resulting polymorph by introducing Sn into the system. By depositing a few-nm thick layer of metallic Sn between two layers of amorphous TiO_2 prepared to yield the *anatase* polymorph of TiO_2, we find that the *rutile* polymorph results if the content of Sn is high enough. If the Sn is introduced as an oxide, no rutile is formed; anatase is by far the predominant phase (with a very small amount of brookite). This observation is consistent with scavenging of oxygen by elemental Sn at the Sn/TiO_2 interfaces, stabilizing the rutile structure which can accommodate oxygen vacancies.

Introduction:

To utilize the material properties of polymorphic functional compounds such as titania, it is important to control the polymorph-selectivity of the synthesis procedure, to understand the limits of stability of the different polymorphs, and for many applications, to find low-temperature routes to the desired polymorph. Titania (TiO_2) is widely used as a catalyst, pigment, structural ceramic, and electronic ceramic and the three common polymorphs, anatase (A-TiO_2), brookite

(B-TiO_2) and rutile (R-TiO_2), all have different properties that can be exploited. Rutile is the thermodynamically stable bulk phase, but in many synthesis processes, anatase is stabilized in nanoparticle form by its low surface energy [1] or by kinetics, and rutile is often reached via the anatase-to-rutile transition [2], usually at temperatures above 600 ˚C. Some studies of TiO_2 nanoparticle powder synthesis have shown that the chemistries used to generate the amorphous precursor can determine which of the TiO_2 polymorphs form upon heating and also influence the subsequent anatase-to-rutile transition [3, 4, 5, 6].

Recently, Mangum *et al*. followed off-stoichiometric routes to stabilize TiO_2 polymorphs in thin-film form, simply by tuning the partial pressure of oxygen ($p(O_2)$) during the deposition of amorphous precursors [7]. Agirseven *et al*. further showed that, along with $p(O_2)$, the sputter deposition rate also affects TiO_2 phase selection [8]. The strong dependence on $p(O_2)$ suggests that oxygen deficiency (relative to TiO_2) in the amorphous precursor drives crystalline polymorph formation. This method produces rutile directly from the amorphous form, bypassing the anatase-to-rutile transition. Oxygen deficiency also affects the anatase-to-rutile transition and the importance of oxygen vacancies in lowering the temperature of this transition has been discussed by Tian *et al*. [9].

Cation doping is another way to manipulate stability ranges of the common polymorphs of TiO_2 [10, 11] and to achieve low-temperature thin film synthesis of both anatase and rutile. The charge state, ionic radius, and substitution position are all factors that can change the anatase-to-rutile transition temperature, which may vary by several hundred degrees [11]. Despite extensive study of these factors, it is still difficult to predict how a particular dopant will impact polymorph stability under different processing conditions. Sn doping, in particular, has been reported both to hinder the formation of rutile [10] and to promote it [12].

Low-temperature rutile formation based on providing a crystalline seed or template to control phase selection have been reported for a variety of processing routes, including work where Sn-containing phases are used as the templates. Trotochaud *et al*. [13] reported a solvothermal method where R-TiO_2 growth was seeded by a cassiterite (C-SnO_2) precursor (which is isostructural to R-TiO_2) resulting in a core/shell nanoparticle structure, whereas a $SnCl_4$ precursor produced a rutile (Sn,Ti)O_2 solid solution. Nie *et al*. [14] observed epitaxial growth of atomic layer deposited R-TiO_2 at 250°C on thermally evaporated C-SnO_2 nanowires. Wang *et al*. [15] also grew R-TiO_2 using C-SnO_2 as a template and Gao *et al*. [16] employed a MnO_2-coated mica substrate as a template to promote the low-temperature formation of R-TiO_2 at 70°C.

In this paper, we report a new method of controlling the polymorph selection when amorphous TiO_2 (a-TiO_2) thin films are annealed, namely introducing a metal Sn layer between two layers of a-TiO_2. The a-TiO_2 with no Sn produces A-TiO_2 upon annealing in air or oxygen. With metal Sn present, this new precursor, upon annealing, turns into A-TiO_2 when the atomic Sn:Ti ratio is less than 7:93 and R-TiO_2 (with some B-TiO_2) when the atomic Sn:Ti ratio is greater than 15:85. The metal Sn oxidizes to C-SnO_2. When Sn is incorporated between the a-TiO_2 layers as an amorphous oxide, only A-TiO_2 results along with C-SnO_2 at any Sn:Ti ratio, with a small amount of B-TiO_2 in some samples.

Our observations suggest that cation doping, seeding, and templating are not as important in the polymorph selection process but rather that the elemental Sn situated in the middle layer of the three-layer stack “scavenges” oxygen from the top and bottom amorphous TiO_2 layers, transforming them into sub-stoichiometric amorphous TiO_2 which favors the rutile polymorph, or brookite in the less extreme cases. When Sn is deposited in the trilayer stack in the presence of an atmosphere providing abundant oxygen during growth, the resulting amorphous tin oxide does not

need to scavenge oxygen from the surrounding a-TiO_2, and annealing yields the anatase polymorph. This processing results in controllable C-SnO_2/R-TiO_2 or C-SnO_2/A-TiO_2 nanoscale heterostructures.

TiO_2/SnO_2 is a system of intense interest with a large literature relating to many different aspects of its materials science and applications. Sn or SnO_2 are logical starting points for additives to TiO_2 because Sn^{4+} is isovalent with Ti^{4+} in this system, R-TiO_2 is isostructural with C-SnO_2 and their ionic radii differ by only about 10% in this charge state and coordination [17].

A large body of work is devoted to producing TiO_2/SnO_2 nanocomposite heterostructures to facilitate improved optical absorption and charge separation for photocatalysis [18]. While evaluating photocatalytic performance is not the focus of our report, the work illustrates a different route to embedding nanoscale SnO_2 in either rutile or anatase.

Metal-induced crystallization (MIC) of amorphous oxides including titania is also a topic of great interest as lowering crystallization temperatures saves energy and is advantageous for materials processing. Bond-breaking in the oxide by the metal is presumed to facilitate the crystallization. Yang et al. [19] report reduced crystallization temperatures in the amorphous to anatase transition when Ni and Cu are introduced. Lermusiaux et al. [20] review this process for several metals in TiO_2; tin is not among them. Our work adds tin to the metals studied in MIC and in particular, it connects the process to oxygen content to produce different polymorphs.

Experiment:

Thin films of a-TiO_2 are deposited by radio-frequency (rf) sputtering of a Ti metal target in an argon (Ar)/oxygen (O_2) atmosphere as described by Agirseven *et al*. [8]. The rf sputter power at the Ti target (100 W) and p(O_2) of 5.45 % are chosen because these conditions produce a-TiO_2 films that crystallize into A-TiO_2 upon subsequent annealing at temperatures greater than 400 ˚C.

Sn is incorporated by sputtering a metal Sn target at 18 W in a pure Ar atmosphere (in which case Sn is deposited as a metal) or an Ar/O_2 atmosphere (in which case Sn is deposited as an oxide). The Sn or SnO_2 is deposited upon an a-TiO_2 film and capped with a similar a-TiO_2 film. Use of a load lock avoids any internal interfaces in the trilayer stack being exposed to atmosphere. By varying the time of the Sn deposition, different Sn contents are achieved in the trilayer structure. The substrate is 2-mm-thick fused SiO_2 (GM Associates 7525-01, 99.99% with the major impurity Al at <19 ppm) or 3-mm diameter Si transmission electron microscopy (TEM) grids with 3 x 3 arrays of 10-nm thick amorphous SiN_x windows (NORCADA, TA301Z); simultaneous deposition on fused SiO_2 and the grids ensures that the deposition conditions are identical for specimens characterized by TEM-based methods and by the other types of characterization. The substrates are at ambient temperature during the deposition. The completed layered structure is annealed in a Neytech Qex high-temperature box furnace. The anneal atmosphere can be vacuum, air, or selected gases; the standard anneal is in air at 500˚C for 30 minutes. To track the annealing process, some samples are annealed for 30 minutes in air at 100˚C intervals up to 500˚C. The film thicknesses are measured after annealing by ellipsometry in a Film-Sense FS-XY150 6-wavelength ellipsometer using a 2-parameter Cauchy model for the refractive index. The system is modeled as a single layer on a fused SiO_2 substrate with the two Cauchy parameters and the film thickness as fitting parameters to the data. This effective medium approach gives good agreement between the index inferred from the experimental data and the index calculated using effective medium theory with refractive indices for SnO_2 and TiO_2 measured from single-composition films deposited using our process [21].

Variations of this deposition procedure are used to test conclusions drawn from measurements of the trilayer structures. Bilayer stacks (Sn upon a-TiO_2), substitution of Au for Sn, and annealing in different atmospheres have yielded useful insights.

Grazing incidence x-ray diffraction (GIXRD) is performed in a Rigaku Ultima IV multipurpose x-ray diffraction system and in a Rigaku SmartLab thin film diffractometer operating at 40 mA and 40 kV using Cu K_α radiation (λ = 1.541 Å, step size = 0.01˚). Raman spectra are collected in a Horiba Jobin-Yvon LabRam 800 Raman spectrometer with a 532-nm laser excitation and a spot size ≈ 1 μm in diameter. Post-acquisition, data are analyzed with the LabSpec 6.0 software suite and compared with reference spectra from the RRUFF database [22] to identify the phases. Electron probe microanalysis (EPMA) is performed in a Cameca SX100 electron microprobe to evaluate the cation composition in the films. Samples are sputter-coated with carbon to eliminate charging. The electron beam diameter is approximately 5 μm and the elemental abundance at three different locations is averaged.

Bright field (BF) TEM images and selected area electron diffraction (SAED) patterns of the thin films deposited on the TEM grids are collected with an FEI Titan (scanning) TEM (STEM/TEM) at an operating voltage of 200 keV. A cross section of a trilayer film with tin deposited as a metal is prepared with a dual-beam focused ion beam/scanning electron microscope (FIB/SEM). Protective carbon and subsequent platinum capping layers are deposited atop the trilayer prior to sectioning with Ga^+ beam. High-angle annular dark field (HAADF) images and energy-dispersive x-ray spectroscopy (EDS) maps are collected in STEM mode.

Results:

Table 1 presents the EPMA-determined cation compositions for representative films where the Sn metal or Sn oxide is deposited for the indicated time, sandwiched between TiO_2 layers each deposited for 80 minutes (4800 s). The compositions are consistent with the larger sputter efficiency of Sn relative to Ti, adjusting for sputter power. The deposition process is mostly stable, producing similar cation ratios for similar depositions for many films, the one exception being samples M07a and M07b in Table 1. The cation ratio measured in a given sample varies less than 0.1 % in three different positions, approximately 1 mm apart. The oxygen content in these films cannot be reliably determined by EPMA because of the overwhelming background presented by the a-SiO_2 substrate. EPMA analysis also cannot distinguish between oxygen in separate layers. A sample of TiO_2/Sn/TiO_2 deposited on Si has EPMA-determined overall oxygen content of the unannealed film consistent with Sn:Ti:O = 0.34:0.66:1.34(2) and of the air-annealed film consistent with Sn:Ti:O = 0.34:0.66:1.97(2). TEM EDS maps the chemical distribution of Sn, Ti and O in the samples. The uncertainty in quantification of oxygen content is high unless the EDS data are compared against a series well-characterized standards with similar and well-defined chemistries, which is beyond the scope of this work. For the purposes of this work, it should be sufficient that the precursors are prepared identically, the a-TiO_2 is close to stoichiometric as deposited, and that the metallic Sn oxidizes upon annealing. The film thicknesses are determined with ellipsometry and range from about 40 - 100 nm. They generally increase with Sn or SnO_2 deposition time, as expected. The film thickness as measured by ellipsometry is in satisfactory agreement with the observed thickness in a TEM cross section, discussed below.

Table 1. Sn:Ti atomic ratios and sample thicknesses for TiO_2/Sn/TiO_2 (M-series) and TiO_2/SnO_2/TiO_2 (O-series) stacks. Sample names indicate whether the middle layer is deposited as a metal (M) or an amorphous oxide (O).

Sample	Sn:Ti	Sn deposition time (s)	Thickness (nm)

M00	0:100	0	42
M02	2:98	15	41
M07a	7:93	60	-
M07b	7:93	75	48
M15	15:85	150	55
M26	26:74	300	75
O14	14:86	150	44
O35	35:65	600	61
O50	50:50	1200	94

We first present the main observations of the "M-series" trilayer films for which Sn is deposited as a metal, followed by parallel observations for the "O-series" trilayer films with Sn deposited as an oxide. Then, we describe additional measurements of the M-series films and other modified configurations that are relevant to the interpretation.

M-series – a-TiO_2/Sn/a-TiO_2 deposition:

Tin is deposited as a metal in the M-series TiO_2/Sn/TiO_2 trilayers. The as-deposited films are shiny and reflective if they have a high Sn content or have a yellowish shade if they have low Sn content when viewed in daylight. All films become transparent in the visible range once annealed (see Figure S1 of the Supporting Information). GIXRD patterns of the as-deposited M-series films in Figure S2 reveal crystalline β-Sn peaks in the Sn:Ti = 15:85 and 24:76 films, which disappear upon annealing. In the Sn:Ti = 2:98 and 7:93 as-deposited films, the Sn content is too low to detect metal peaks with our x-ray diffractometer, and only the amorphous substrate signal appears for those two concentrations.

The pure TiO_2 film is amorphous as deposited and crystallizes into the anatase polymorph A-TiO_2 upon annealing with no trace of the rutile polymorph R-TiO_2 evident in either the GIXRD pattern or the Raman spectrum (bottom traces of Figure 1(a) and 1(b), respectively), all of which is consistent with the work by Agirseven et al. [8]. The GIXRD patterns and Raman spectra of the annealed M-series films in Figure 1 show that films with Sn:Ti = 2:98 and 7:93 also crystallize

into A-TiO_2. X-ray peaks at 2θ ~ 25.4˚, 48.2˚, and the doublet near 55.1˚ are signatures of anatase, as is the pattern of Raman modes at 145 cm^{-1} (E_g), 399 cm^{-1} (B_{1g}), 519 cm^{-1} (A_{1g} and B_{1g}) and 638 cm^{-1} (E_g). In sharp contrast, films with a higher tin content, Sn:Ti: = 15:85 and 26:76, show predominantly R-TiO_2 and C-SnO_2 in GIXRD. Broad Raman peaks at 440 cm^{-1} (E_g) and 636 cm^{-1} (A_{1g}) also indicate the presence of R-TiO_2 [22].

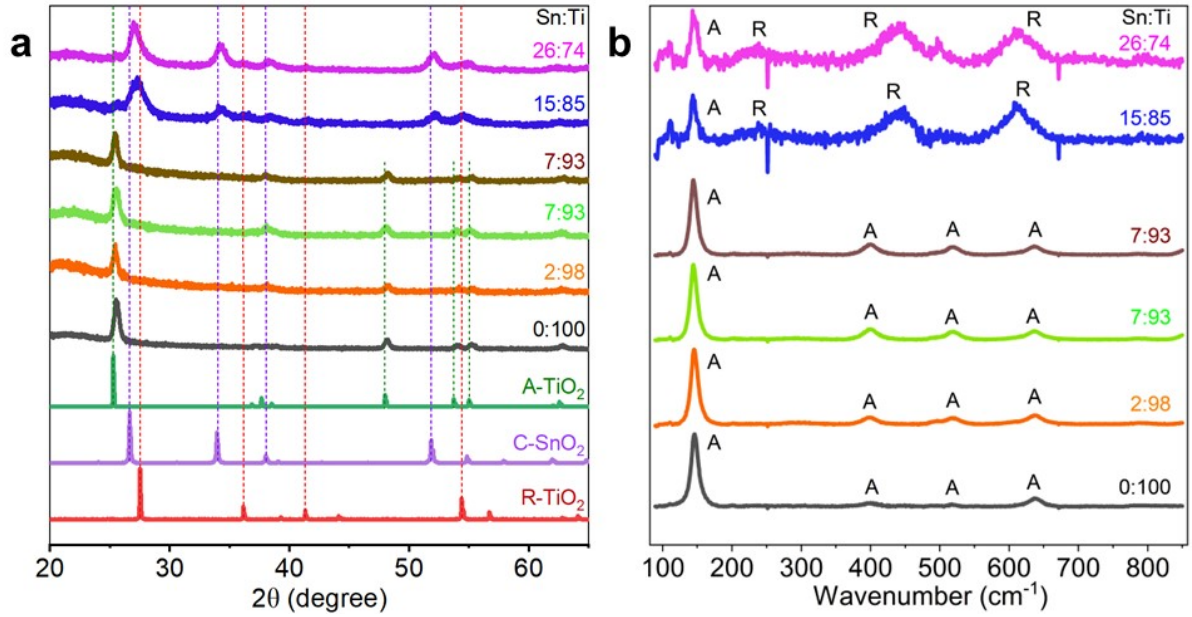

Figure 1. GIXRD patterns (a) and Raman spectra (b) of the air-annealed trilayer films (M-series, deposited as a-TiO_2/Sn/a-TiO_2). Both show R-TiO_2, rather than A-TiO_2, forms when Sn:Ti ≥ 15:85. All patterns and spectra are normalized to the largest peak and the substrate signal is subtracted from the Raman spectra.

While the crystallization of a-TiO_2 to A-TiO_2 in the low Sn-content films and to R-TiO_2 in the higher Sn-content films is the most striking feature of the GIXRD and Raman analyses, it is important to point out the observation of minor phases and the lack of signal of certain expected phases, which become significant in the discussion of the TEM observations below. First, the 15:85 and 24:76 films have a significantly reduced XRD peak near 2θ = 25.4˚ and a similarly reduced Raman peak at 150 cm^{-1}, which are consistent with a reduction in A-TiO_2, but which could also be interpreted as the appearance of B-TiO_2, as we discuss below. Second, C-SnO_2 is not evident in

the 2:98 and 7:93 films in GIXRD, but it is detected in SAED from which we conclude that the x-ray scattering power of Sn is too weak to be detected by GIXRD at these contents. We see only a very weak Raman signature of C-SnO_2 even in pure SnO_2 films with strong XRD peaks, so the absence of a Raman signature in the films with SnO_2 as a minority phase seems reasonable.

Figure 2(a-c) shows plan-view TEM images of the as-deposited M-series thin films, which consist of amorphous TiO_2 and crystalline β-Sn, as identified by analysis of the SAED patterns in Figure S3(a-c) of the Supporting Information. The as-deposited films appear inhomogeneous and are covered with discrete cell-like nanostructures with dark centers. The centers are identified as β-Sn by a combination of SAED (Figure S3) and TEM EDS shown in Figure S4 of the Supporting Information. The size of the Sn nanograins increases with increasing Sn content. Some of the Sn nanograins are darker than others due to the Bragg diffraction conditions being met by certain orientations of the Sn. The distribution of Sn and Ti in the TEM EDS (Figure S4) and the appearance of light rings around the dark β-Sn may be explained by dewetting of the Sn layer from the first layer of a-TiO_2, which is then capped by the top layer of a-TiO_2.

Figure 2(d-f) shows the M-series films after annealing at 500°C for 30 min in air. A-TiO_2, R-TiO_2 and C-SnO_2 are identified by the analysis of the electron diffraction data shown as indexed rotational averages in Figure 3 (the raw SAED patterns are in Figure S3(d-f)). There is no evidence of remaining metallic tin. After annealing, the films retain the cellular nanostructure apparent in the as-deposited samples. TEM EDS (Figure S4) shows that the Sn is still localized in cassiterite grains and has not diffused significantly in the plane of the film. Some of the grains in the post-annealed samples have alternating dark and light stripes (apparent in the center of Figure 2e) which is a moiré pattern caused by overlapping crystalline grains.

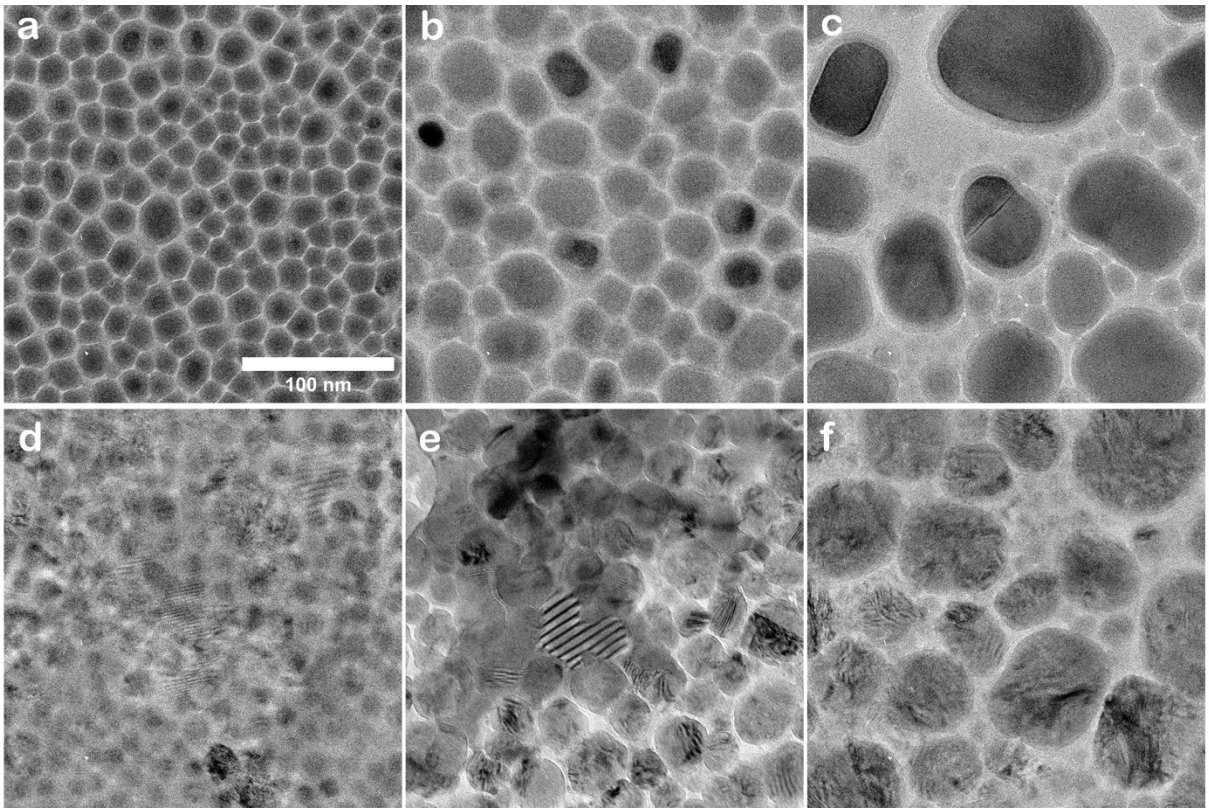

Figure 2. Bright field TEM images of the M-series trilayer films as-deposited (a-c) and after annealing in air at 500°C for 30 min (d-f), where (a) and (d) are deposited with a 7:93 Sn:Ti ratio, (b) and (e) with 15:85, and (c) and (f) with 26:74. All images are shown to the same scale.

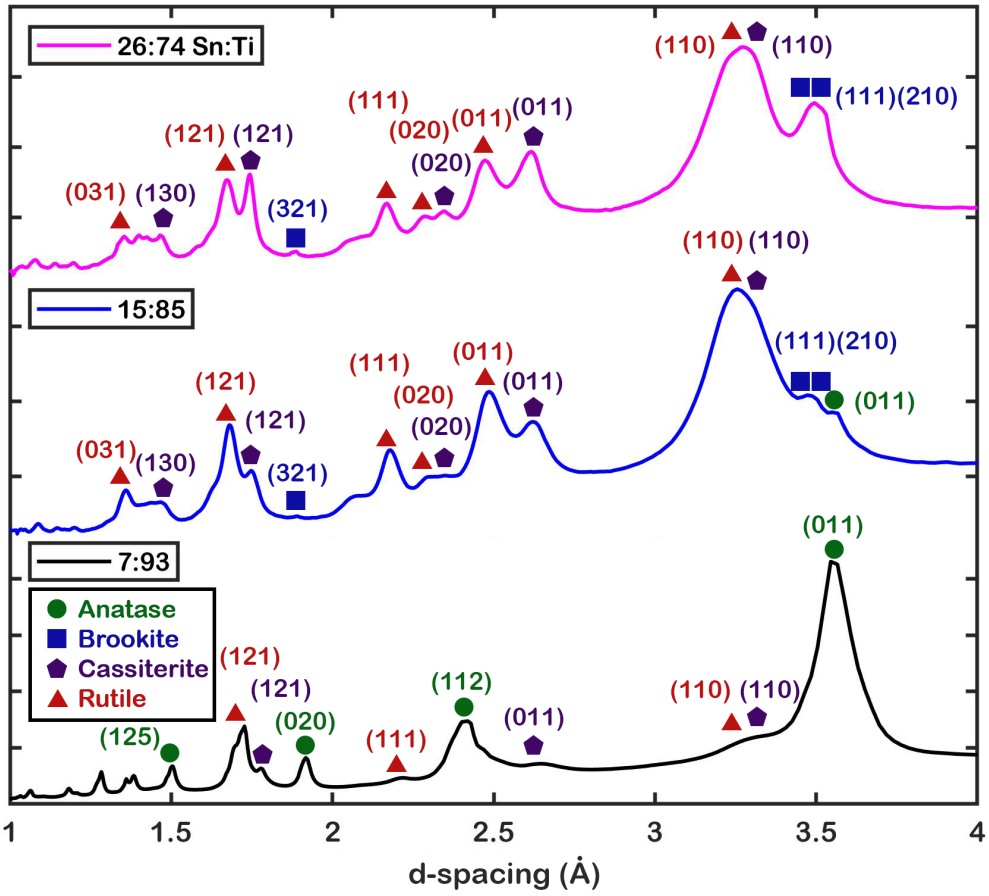

Figure 3. Rotational averages of the intensities of the SAED patterns (converted to real-space units) of M-series air-annealed trilayer films with 7:93, 15:85 and 26:74 Sn:Ti ratios.

Figure 3 shows rotational averages of the SAED pattern intensities (Figure S3(d-f) of the Supporting Information) for M-series films with Sn:Ti ratios of 7:93, 15:85 and 26:74. The indexed peaks confirm the results of the GIXRD in Figure 1, in which the primary phases are A-TiO_2 in the 7:93 film and R-TiO_2 and C-SnO_2 in the 15:85 and 26:74 films. The SAED shows the presence of B-TiO_2 in the films with the 15:85 and 26:74 ratios and possibly anatase in the 15:85 film, which is not conclusive in the GIXRD data. Likewise, SAED is sensitive enough to detect the presence of the expected C-SnO_2 in the 7:93 film. A small amount of R-TiO_2 is also apparent in SAED of this film, which could be due to the tendency of rutile to form on inhomogeneities and defects.

The presence of metal Sn nanograins in the as-deposited M-series trilayer films is further confirmed by high-resolution transmission electron microscopy (HRTEM) images of the as-

deposited and annealed films; an example, M07b with Sn:Ti = 7:93, is in Figure 4(a). The crystal planes are evident and the measured lattice spacing of the darker Sn for this as-deposited sample is 2.75 Å, consistent with the d_{101} plane of tetragonal β-Sn. The HRTEM image of the annealed version of M07b in Figure 4(b) reveals lattice planes with spacing 3.49 Å, consistent with the d_{110} plane of C-SnO_2.

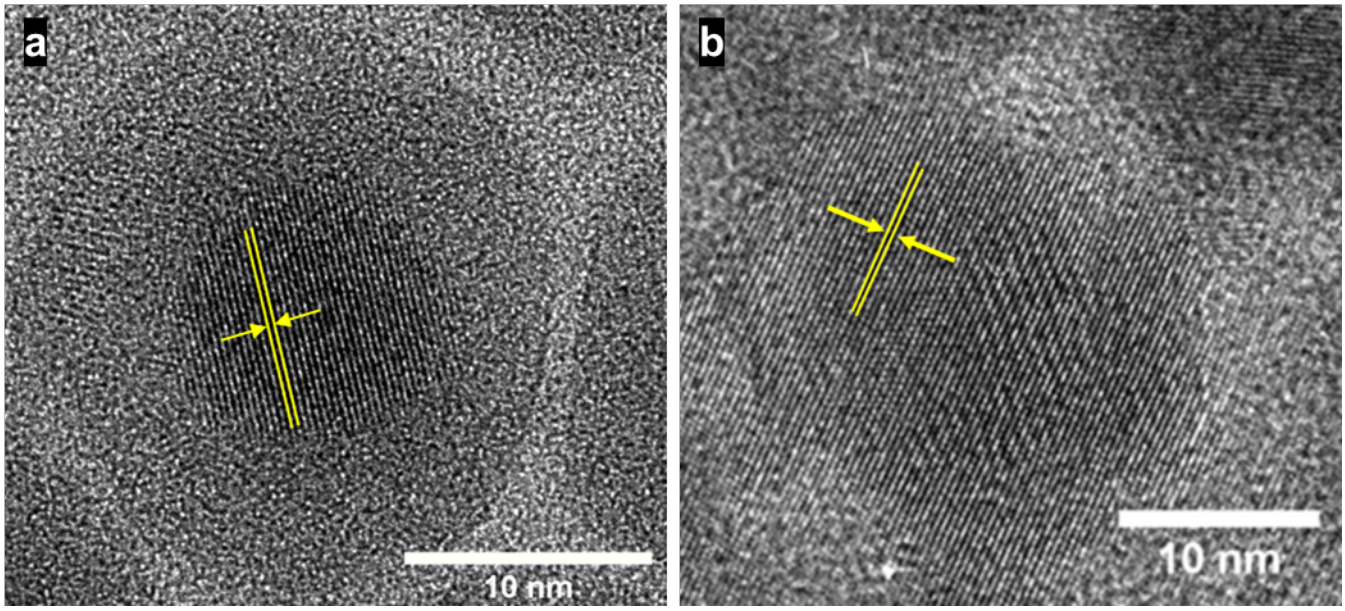

Figure 4. HRTEM image of M-series trilayer M07b with Sn:Ti = 7:93 (a) as deposited, (b) air-annealed.

Figure 5 shows a STEM HAADF image and STEM/EDS mapping of a cross section of the air-annealed M-series trilayer with Sn:Ti = 15:85. The HAADF STEM image clearly shows the morphology of the tin oxide layer. The EDS mapping shows that there is no significant diffusion of tin into titania and that the trilayers remain distinct. The oxygen is fairly uniform across the trilayers (Figure S5(a) has a mapping of oxygen alone), and is a minor component in the substrate and capping layers (Figure S5 (b)). Because the roughness of the SnO_2 layer is transferred to the

conforming upper TiO_2 layer, the top interface between TiO_2 and the carbon capping layer is not resolved.

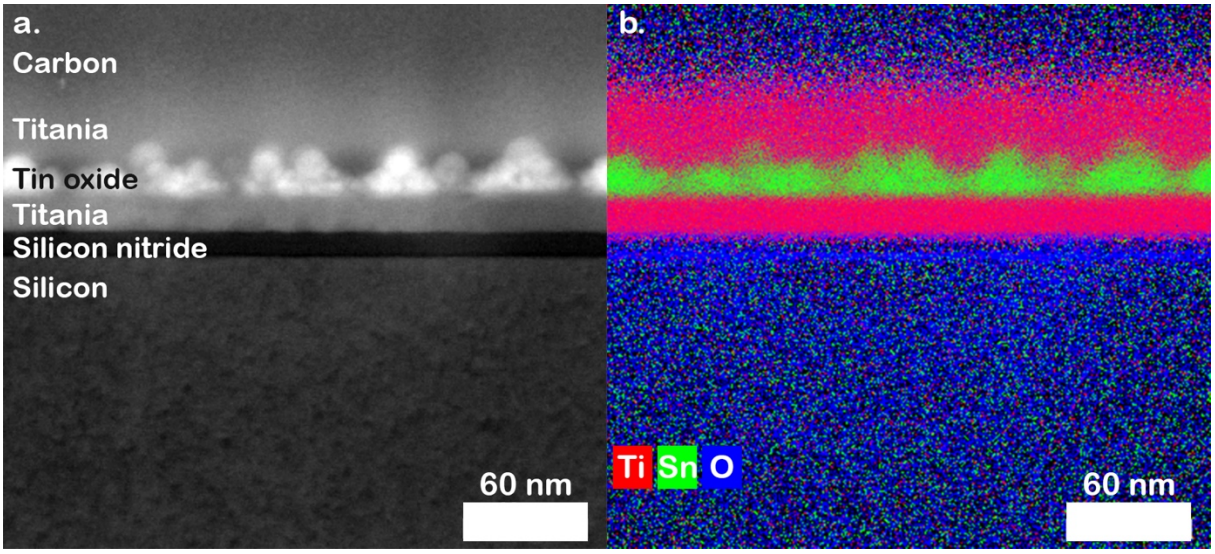

Figure 5. (a) STEM HAADF image of a cross section of an air-annealed M-series trilayer film with Sn:Ti = 15:85. (b) STEM/EDS mapping of Sn, Ti and O of the area shown in (a).

O-Series: a-TiO_2/a-SnO_2/a-TiO_2 deposition:

Tin is deposited as an oxide in the O-series TiO_2/SnO_2/TiO_2 films. All films appear transparent as deposited and do not change appearance significantly once annealed. GIXRD patterns of the as-deposited O-series trilayer (Figure S6) show only amorphous material, and no metallic Sn.

The GIXRD patterns and Raman spectra of the air-annealed O-series films are presented in Figure 6. For all three samples, x-ray peaks and Raman peaks indicate the presence of A-TiO_2. For samples O35 (Sn:Ti = 35:65) and O50 (Sn:Ti = 50:50) the (110), (101), and (211) peaks of C-SnO_2 indicate that SnO_2 is also present along with A-TiO_2. It is important that *no R-TiO_2* is observed in any sample, irrespective of the Sn content (peaks would be expected at $2\theta = 37°$ and 42°; c.f. Figure 1). This differs significantly from the M-series depositions where at high Sn content, R-TiO_2 is seen.

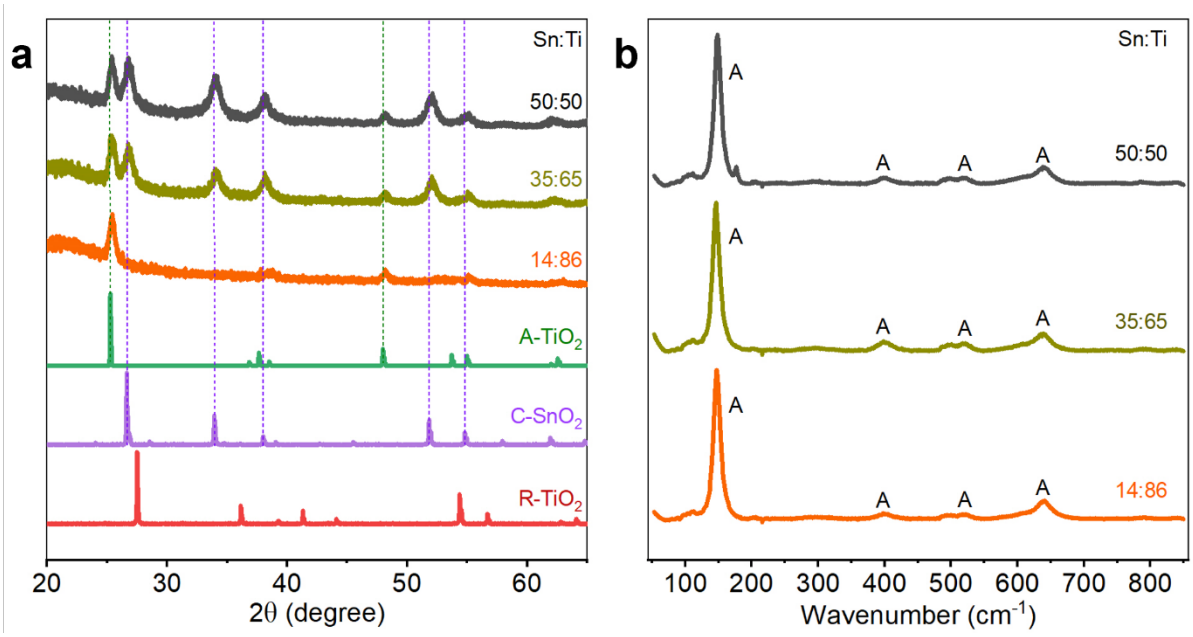

Figure 6. GIXRD patterns (a) and Raman spectra (b) of the O-series air-annealed $TiO_2/SnO_2/TiO_2$ trilayer films.

TEM images from the O-series trilayer film O50 are shown in Figure 7. Comparing the morphology of the as-deposited O-series film in Figure 7(a) with the TEM micrographs of M-series films in Figure 2(a), (b) and (c), it is evident that SnO_2 and TiO_2 form more uniform layers when the middle layer is deposited as amorphous tin oxide instead of metallic tin. The broad, diffuse rings in the SAED pattern in Figure 7(a) confirm that the as-deposited sample is amorphous, whereas the narrow rings and sharp spots in Figure 7(b) indicate that the air-annealed sample is polycrystalline. Figure 7(c) presents the rotationally averaged of the annealed film in Figure 7(b), demonstrating the presence of A-TiO_2 and C-SnO_2 and some B-TiO_2.

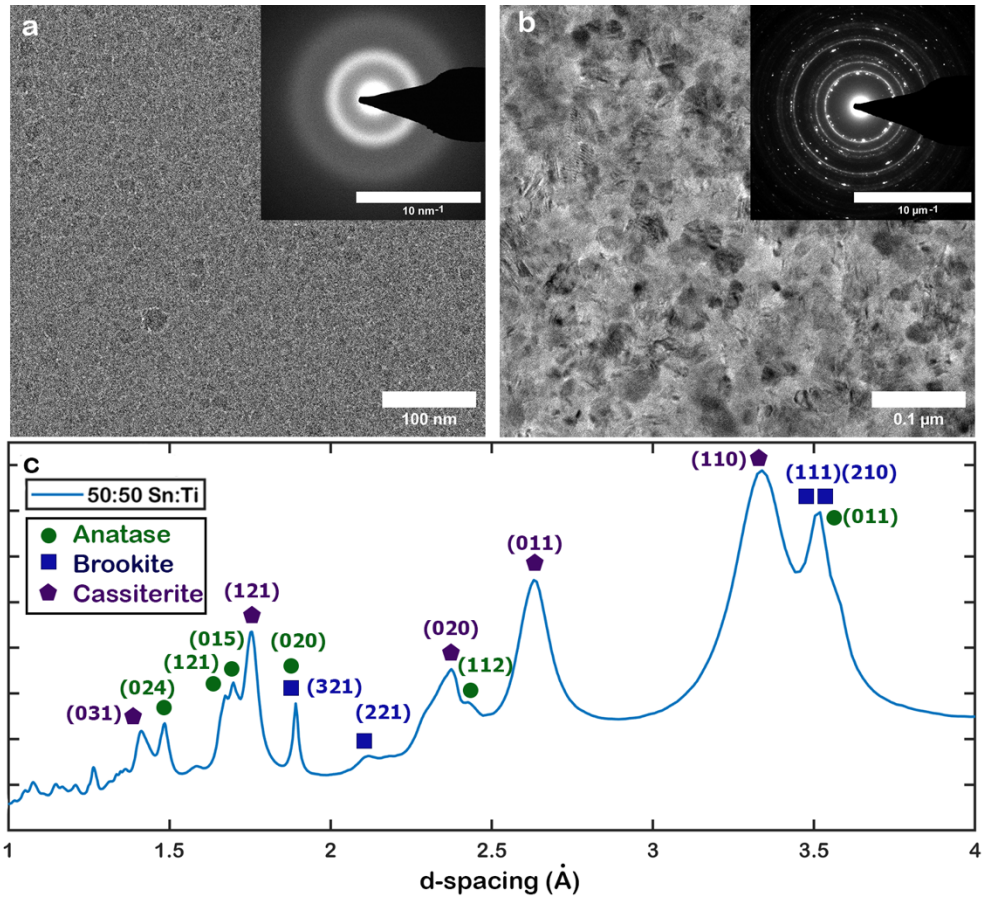

Figure 7. TEM image and SAED pattern (inset) of the trilayer O-series film O50 with Sn:Ti = 50:50, as-deposited (a) and air-annealed (b). Rotational average (c) of the inset diffraction pattern intensity of the air-annealed film.

SIMS measurements (Figure S7) probe the cross section of the O-series and M-series films and are consistent with the in-plane observations by TEM: Sn and SnO_2 are confined between the TiO_2 layers, where they were initially deposited.

Bilayer M-series films (TiO_2/Sn deposition):

GIXRD patterns of bilayer films prepared and annealed in the same fashion as the M-series trilayer films, but without the top a-TiO_2 layer, are shown in Figure 8. As in the case of the trilayer structures, the a-TiO_2 crystalizes to A-TiO_2 at low Sn content, and to R-TiO_2 at high Sn content, and C-SnO_2 forms in all cases. The difference is that the transition in final polymorph from anatase to rutile occurs at a higher Sn:Ti ratio. For example, in a bilayer structure with Sn:Ti = 19:81, only

A-TiO_2 and C-SnO_2 are present, while in a trilayer of comparable composition (e.g. M15 with Sn:Ti = 15:85), R-TiO_2 and C-SnO_2 are present but no A-TiO_2 (cf. Figure 1). In a bilayer structure with Sn:Ti = 32:68, A-TiO_2 is no longer present and R-TiO_2 and C-SnO_2 crystallize with a pattern with features similar to M14 (Sn:Ti = 14:76). In the bilayer sample with the highest Sn:Ti ratio (48:52), a small amount of metallic β-Sn remains after annealing, and in this case, a small amount of A-TiO_2 can be detected.

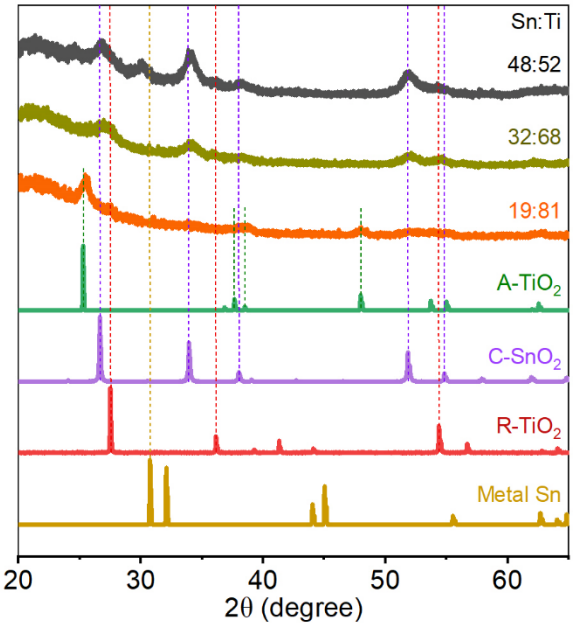

Figure 8. GIXRD patterns of air-annealed bilayer films (deposited as substrate/Sn/a-TiO_2).

Variable temperature and variable atmosphere annealing of M-series trilayer films:

Figure 9 (a) and (b) present GIXRD patterns of M-series trilayer films annealed in air at 200˚C, 300˚C and 400˚C for 30 minutes (25˚C, 500˚C not shown) and Figure 9(c) presents the crystallization temperature, defined by the first appearance of the prominent peak near 25˚ for A-TiO_2 and 27˚ for R-TiO_2.

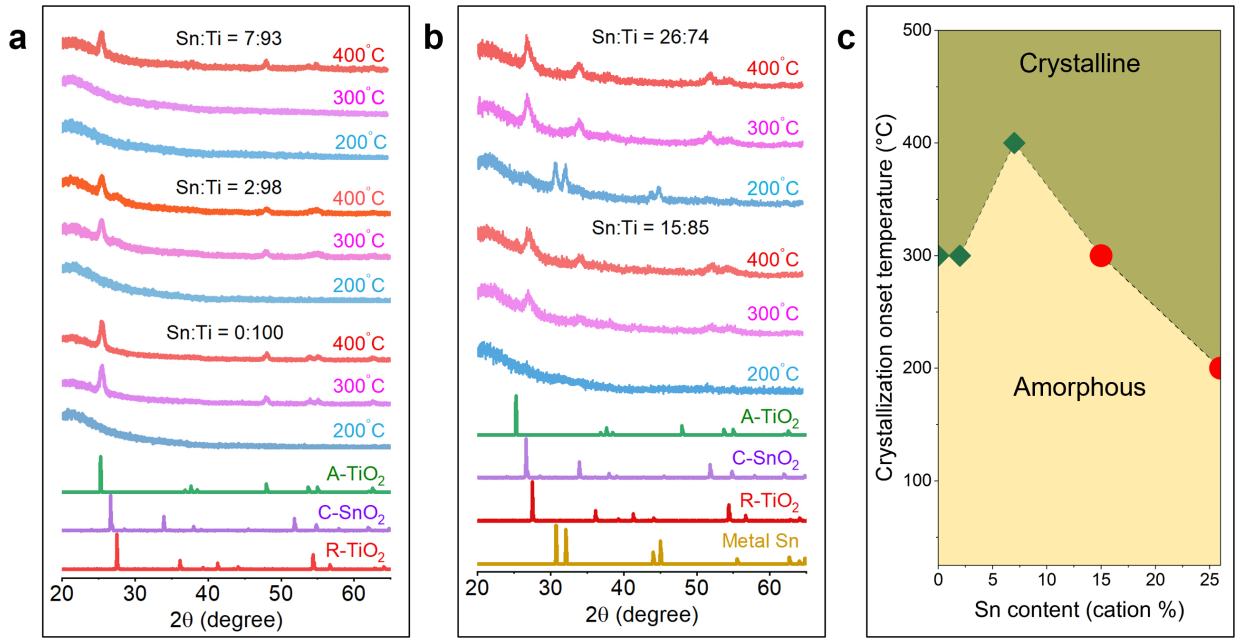

Figure 9: GIXRD patterns from the variable-temperature study of air-annealed M-series films: (a) Sn:Ti = 0:100 (M00), Sn:Ti = 2:98 (M02), Sn:Ti =,7:93 (M07b); (b) Sn:Ti = 15:85 (M15), Sn:Ti = 26:74 (M26). (c) Crystallization onset temperature as a function of Sn content. The dominant crystalline phase is anatase (green diamonds) at low Sn concentration or rutile (red circles) at high Sn concentration.

As the annealing temperature is increased, any metal Sn disappears, as expected, and crystalline oxides form: A-TiO_2 in M00, M02, M07b and R-TiO_2 in M15 and M26 and, where the Sn content is high enough to detect it, C-SnO_2. For samples M00 (with no Sn) and M02 (Sn:Ti = 2:98) A-TiO_2 first appears at 300˚C, and the crystallization temperature increases to 400˚C for sample M07b (Sn:Ti = 7:93) with higher Sn content. The temperature trend reverses for the two samples where R-TiO_2 appears at 300˚C for sample M15 (Sn:Ti = 15:85) and at 200˚C for sample M26 (Sn:Ti = 26:74).

The GIXRD patterns in Figure 10 are from a variable anneal atmosphere study of M-series films prepared with the Sn:Ti = 26:74 protocol. Each film is divided and part is annealed in air (as a control), part in O_2, and part in Ar, all at 500 ˚C. The air- and the O_2-anneal produce the same

pattern; only R-TiO_2 and C-SnO_2 peaks appear. The Ar-anneal produces A-TiO_2 in addition to R-TiO_2 and C-SnO_2.

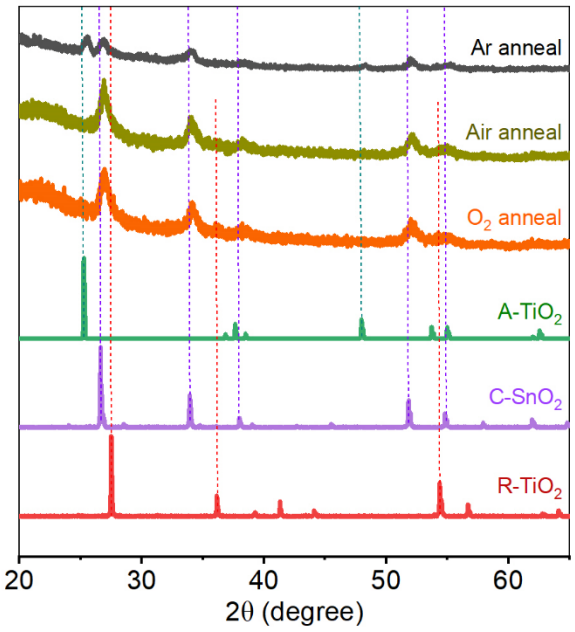

Figure 10: GIXRD patterns of M-series films prepared with the Sn:Ti = 26:74 protocol and annealed in air, O_2, and Ar at 500˚C.

Discussion:

The M-series trilayer depositions with metallic Sn demonstrate that amorphous TiO_2 deposited in such a way as to crystallize into the *anatase* structure upon annealing can be induced to crystallize into the *rutile* structure by incorporating a layer of metallic β-Sn in the precursor film. There is a critical ratio of Sn:Ti between 7:93 and 15:85 below which anatase forms, and above which rutile forms (with possibly small amounts of brookite). At all Sn contents, β-Sn oxidizes to cassiterite SnO_2 which remains as a second phase distributed as SnO_2 grains on the 20 – 100 nm scale due to dewetting of the Sn when deposited on the a-TiO_2. The presence of *metallic* Sn in the precursor is critical to the formation of R-TiO_2 as evidenced by the fact that when any

amount of Sn is incorporated as an *oxide* in the same trilayer deposition mode, *no* R-TiO_2 is formed. Primarily A-TiO_2 is formed with some B-TiO_2.

We know from the work of Mangum [7], Haggerty [23] and Agirseven [8] that amorphous TiO_2 precursor films crystallize into the rutile polymorph when deposited at very low $p(O_2)$, brookite at intermediate $p(O_2)$ and anatase at the highest $p(O_2)$. These observations are valid for films generated both by pulsed laser deposition and rf sputtering. We therefore suggest that the oxidation of the embedded β-Sn in the trilayer structures locally reduces the amorphous TiO_2, effectively "scavenging" oxygen from the precursor film. If there is sufficient Sn, then the titania may be sufficiently depleted of oxygen to induce the formation of rutile in a precursor that would have formed anatase in the absence of Sn. Supporting experimental evidence comes from the bilayer M-series films whose GIXRD patterns are presented in Figure 8. In these structures, A-TiO_2 crystallization persists until at least Sn:Ti = 19:81, whereas in the trilayer structures, A-TiO_2 crystallization has already been suppressed at a smaller tin content (Sn:Ti = 15:68). In the bilayer structures, the metallic Sn layer is exposed directly to the ambient atmosphere and the Sn obtains the requisite oxygen to form C-SnO_2 from the atmosphere and from the a-TiO_2 layer below. It is therefore reasonable that the scavenging process is less efficient than when Sn is capped by a-TiO_2 as in the trilayer case. More Sn is needed in the bilayer case to scavenge enough oxygen to induce R-TiO_2 crystallization.

Shannon and Pask show that the transformation of anatase to rutile TiO_2 [2] is accelerated by annealing in low-pO_2 atmospheres; they suggest that oxygen vacancies are introduced and that the resulting Ti-O bond breaking facilitates the volume collapse necessary to convert from anatase to rutile. The amorphous "anatase precursor" prepared in the films in our study is likely locally similar to crystalline anatase, so Shannon and Pask's argument could hold in this case, too: if the

β-Sn scavenges oxygen and induces oxygen vacancies in the amorphous TiO_2 precursor, then the rutile form is likely to crystallize.

One might argue that Sn cannot reduce or scavenge oxygen from titania based of the lower energy of formation of TiO_2 ($\Delta_fH^\circ_{rutile}$= -945 kJmol^{-1}; $\Delta_fH^\circ_{anatase}$= -939 kJmol^{-1}) [24] relative to SnO_2 (Δ_fH°= -578 kJmol^{-1}[25]) or even SnO (Δ_fH° = -281 kJmol^{-1} [25]). However, what may be more relevant is the very low energies of formation of the reduced oxides of titanium (Δ_fH° = -1521, -2459 and -3405 kJmol^{-1} for Ti_2O_3, Ti_3O_5 and Ti_4O_7, respectively [24]), which suggest a strong driving force to release oxygen when there is a proximate oxidizable metal. Our preliminary experiments with a gold layer replacing the tin layer yielded gold metal peaks and no crystalline TiO_2, or at most a very weak signature of A-TiO_2 (Figure S8). This observation is similar to that of Mosquera *et al*. who observed that anatase formation from an amorphous precursor was inhibited when Ag metal nanoparticles were incorporated in the precursor [26]. Au and Ag are both very unlikely to form oxides so the similar behavior is expected.

The fact that we observe brookite (along with rutile) in the SAED patterns of some annealed M-series films (Figure 3) and brookite (along with anatase) in some of the O-series films (Figure 7) is consistent with the argument that the presence of Sn induces a locally reduced oxygen environment. In the M-series annealing, the Sn metal scavenges oxygen from the a-TiO_2 producing regions of strong to medium local oxygen deficiency in the TiO_2, resulting in rutile and brookite. In the O-series trilayer deposition method where Sn is incorporated as oxide, scavenging would be driven only by any oxygen deficiency in the SnO_{2-x}. As a result, the amorphous TiO_2 precursor film retains almost all the oxygen incorporated during deposition or at most has a medium oxygen deficiency and anatase and a little brookite are obtained upon annealing.

When the role of the annealing atmosphere is also considered (Figure 10), the picture becomes more complicated. When a high-Sn content M-series trilayer is annealed in O_2, R-TiO_2 (and C-SnO_2) are observed, just as in the air-annealed case described above. But when the same structure is annealed in Ar, A-TiO_2 (and C-SnO_2) result. At first, this result may seem contradictory. The oxygen to form cassiterite SnO_2 can come only from the TiO_2, so why does rutile not form? Shannon and Pask [2] demonstrate that the anatase-to-rutile transition is *inhibited* by vacuum annealing; he suggests that in this case Ti interstitials are formed, leaving the remaining Ti locally fully coordinated in the anatase structure with no Ti-O bond breaking to facilitate the volume collapse. It is less clear that the Ar anneal in our case is analogous to the vacuum anneal in Shannon and Pask's work, but it does provide a plausible hypothesis that could be tested, though it is beyond the scope of this paper.

One alternative explanation to the proposed oxygen-scavenging by Sn to promote rutile formation that may be ruled out by these experiments is that the R-TiO_2 growth is templated or seeded by the C-SnO_2, as observed for example by Wang et al. [15]. First, in the O-series experiments where tin is deposited as an oxide in the middle layer, that C-SnO_2 would be expected to have seeded R-TiO_2, but it did not. Second, Figure 9 tracks the crystallization as the temperature is increased and in the high Sn-content films, R-TiO_2 appears simultaneously with C-SnO_2 and A-TiO_2 does not form at all. In the seeding or templating scenario, it might be expected that C-SnO_2 would form before R-TiO_2, or that A-TiO_2 might nucleate and grow in the regions away from C-SnO_2.

A second observation from Figure 9 is that the incorporation of metallic Sn reduces the crystallization temperature for R-TiO_2 but increases it for A-TiO_2, although the temperature resolution is coarse. Similar trends are observed by Mosquera et al. [26] who incorporate Ag

nanoparticles in a-TiO_2. Their argument that the steric effects of the metal nanoparticles inhibit diffusion to delay the crystallization of anatase and to limit the free volume to enhance rutile formation may also be relevant in the Sn case. In addition, the scavenging mechanism postulated here could also lower the R-TiO_2 crystallization temperature. More Sn would induce more vacancies in a-TiO_2 and introduce unsaturated Ti-O bonds in the amorphous network that could facilitate the restructuring required for crystallization, which could then occur at lower temperatures.

Conclusion:

We have observed that introducing metallic Sn into amorphous a-TiO_2 films results in the TiO_2 crystallizing into the rutile polymorph R-TiO_2 when the Sn content is high enough. The a-TiO_2 crystallizes into the anatase polymorph A-TiO_2 in the absence of metallic Sn but deposited under otherwise identical conditions. Metallic Sn is critical; if the Sn is introduced as an (amorphous) oxide, the a-TiO_2 still crystallizes into A-TiO_2. In this regard, changing the metallic Sn content seems to mimic the action of varying the pO_2 during the deposition of a-TiO_2 – namely that rutile (and in some cases brookite) crystallizes upon annealing of high-Sn / low pO_2 amorphous films and anatase crystallizes upon annealing of low-Sn / high pO_2 films. We suggest that the presence of an oxidizable metal (even one, like Sn, whose oxide has a higher formation energy than TiO_2) results in oxygen being scavenged by elemental Sn at the Sn/TiO_2 interfaces. The local reduction of oxygen in the a-TiO_2 precursor then produces a "low pO_2" environment which then accommodates oxygen vacancies. These vacancies could provide the necessary atomic mobility for the Ti-O bonds to rearrange into the dense structure required for R-TiO_2 from the more open, less dense structure of A-TiO_2. The metallic Sn is oxidized into cassiterite or C-SnO_2 during

this process and the C-SnO_2 remains as discrete nanoscale grains dispersed in the TiO_2 matrix. This nanoscale structure could be the basis for creating capacitive devices with different dielectric constants and understanding the TiO_2/SnO_2 interface that might be useful in photocatalysis, solar cells, gas sensors or batteries. Introduction of metallic Sn into a-TiO_2 provides a means to select the polymorph that results upon crystallization and to vary the crystallization temperature.

Supporting Information

Representative 400-900 nm transmission and reflection spectra, GIXRD patterns for as-deposited films, SAED patterns of all M-series films before and after annealing, HAADF STEM and EDS images for selected M-series films, cross-sectional STEM/EDS of a representative annealed M-series film, SIMS depth profiles for selected M- and O-series films and GIXRD patterns of M-series films with Au substituted for Sn. All information in PDF format.

Corresponding Author

Janet Tate, Department of Physics, 301 Weniger Hall, Oregon State University, Corvallis, Oregon 97331, USA.

Acknowledgements

Effort by T.D.K. was supported by the National Science Foundation, Division of Materials Research CER [Grant No. 1945520]. Effort by P.B. was supported by the Lundeen Fund from the College of Science, Oregon State University. TEM was performed at the Oregon State University Electron Microscope Facility which is supported by NSF MRI Grant No. 1040588, the Murdock Charitable Trust, and the Oregon Nanoscience and Micro-Technologies Institute. We gratefully acknowledge the assistance of Dr. Peter Eschbach with the FIB specimen preparation. Film deposition and/or characterization facilities included the Oregon State University Materials

Synthesis and Characterization Facility, the Oregon State University X-Ray Diffraction Facility, the Rorrer Laboratory, and CAMCOR. The ToF-SIMS experiment was performed on a project award (DOI: 10.46936/cpcy.proj.2023.60681/60008771) from the Environmental Molecular Sciences Laboratory, a DOE Office of Science User Facility sponsored by the Biological and Environmental Research program under Contract No. DE-AC05-76RL01830. Measurements were performed and analyzed by Dr. Binod Paudel and Jeffrey Arul Dhas of Pacific Northwest National Laboratory.

References:

1. Ranade, M. R.; Navrotsky, A.; Zhang, H. Z.; Banfield, J. F.; Elder, S. H.; Zaban, A.; Borse, P. H.; Kulkarni, S. K.; Doran, G. S.; Whitfield, H. J. Energetics of Nanocrystalline TiO_2, PNAS 2002, 99, 6476–6481.
2. Shannon, R.D.; Pask, J.A. Kinetics of the Anatase-Rutile Transformation. J. Am. Ceram. Soc. 1965, 48, 391–398.
3. Tang, J.; Redl, F.; Zhu, Y.; Siegrist, T.; Brus, L. E.; Steigerwald, M. L. An Organometallic Synthesis of TiO_2 Nanoparticles, Nano Lett. 2005, 5, 543–548.
4. Niederberger, M.; Bartl, M. H.; Stucky, G. D. Benzyl Alcohol and Titanium Tetrachloride - A Versatile Reaction System for the Nonaqueous and Low-Temperature Preparation of Crystalline and Luminescent Titania Nanoparticles, Chem. Mater. 2002, 14, 4364–4370.
5. Ovenstone, J.; Yanagisawa, K. Effect of Hydrothermal Treatment of Amorphous Titania on the Phase Change from Anatase to Rutile during Calcination. Chem Mater. 1999, 11, 2770–2774.

6. Coronado, D. R.; Gattorno, G. R.; Pesqueira, ME.E.; Cab, C.; Coss, R.D.; Oskam, G. Phase-pure TiO_2 Nanoparticles: Anatase, Brookite and Rutile. Nanotechnology 2008, 19, 63389-63399.
7. Mangum, J.S.; Agirseven, O.; Haggerty, J.E.S.; Perkins, J.D.; Schelhas, L.D.; Kitchaev, D.A.; Garten, L.M.; Ginley, D.S.; Toney, M.F.; Tate, J.; Gorman, B.P. Selective Brookite Polymorph Formation Related to the Amorphous Precursor State in TiO_2 Thin Films. J. Non-Cryst. Solids 2019, 505, 109–114.
8. Agirseven, O; Rivella Jr., D.T.; Haggerty, J.E.S.; Berry, P.O.; Diffendaffer, K.; Patterson, A.; Kreb, J.; Mangum, J.S.; Gorman, B.P.; Perkins, J.D.; Chen, B.R.; Schelhas, L.T.; Tate, J. Crystallization of TiO_2 Polymorphs from RF-Sputtered, Amorphous Thin-Film Precursors, AIP Adv. 2020, 10, 025109.
9. Tian, Z.; Du, S.; Cheng, X.; Zhang, J.; Li, F.; Chen, Z.; Lv, Y.; Zhu, Y.; Liu, G. The Role of Oxygen Vacancy in Anatase to Rutile Transformation of TiO_2, Cryst. Growth Des. 2022, 22, 6852−6856.
10. Toledo-Antonio, J. A.; Pedraza, F.; Bokhimi, X. The Effect of Doping Low Temperature Rutile with Tin, J. New Mater. Electrochem. Systems 2005, 8, 85– 90.
11. Vargas, S.; Arroyo, R.; Haro, E.; Rodríguez. R. Effects of Cationic Dopants on the Phase Transition Temperature of Titania Prepared by the Sol-Gel Method. J. Mater. Res. 1999, 14, 3932–3937.
12. Oropeza, F. E.; Davies, B.; Palgrave, R. G.; Egdell, R. G. Electronic Basis of Visible Region Activity in High Area Sn-doped Rutile TiO_2 Photocatalysts, Phys. Chem. Chem. Phys., 2011, 13, 7882–7891.

13. Trotochaud, L.; Boettcher, S.W. Synthesis of Rutile-Phase $Sn_xTi_{1-x}O_2$ Solid-Solution and $(SnO_2)_x/(TiO_2)_{1-x}$ Core/Shell Nanoparticles with Tunable Lattice Constants and Controlled Morphologies, Chem. Mater. 2011, 23, 4920-4930.

14. Nie, A.M.; Liu, J. B.; Li, Q. Q.; Cheng, Y.C.; Dong, C.Z; Zhou, W; Wang. P; Wang, Q.X.; Yang, Y.; Zhu, Y. H.; Zeng, Y. W.; Wang, H. T. Epitaxial TiO_2/SnO_2 Core–Shell Heterostructure by Atomic Layer Deposition, J. Mater. Chem. 2012, 22, 10665–10671.

15. Wang, H.; Xu, S.; Gordon, R.G. Low Temperature Epitaxial Growth of High Permittivity Rutile TiO_2 on SnO_2, *Electrochem. Solid-State Lett.* 2010, 13, G75-G78.

16. Gao, Q.; Wu, X.; Fan, Y.; Zhou, X. Low-Temperature Synthesis and Characterization of Rutile TiO_2-Coated Mica-Titania Pigments, Dyes Pigm. 2012, 95, 534–539.

17. Shannon, R. D.; Prewitt, C. T.; Effective Ionic Radii in Oxides and Fluorides, Acta Cryst. B25 (1969) 925-946.

18. Rajput, B. R.; Jamble, S. N.; Kale R. B.; A review on TiO_2/SnO_2 heterostructures as a photocatalyst for the degradation of dyes and organic pollutants Journal of Environmental Management 307 (2022) 114533.

19. Yang, C.; Hirose, Y.; Nakao, S.; Huong, N. L. H.; Hasegawa, T.; Metal-induced solid-phase crystallization of amorphous TiO_2 thin films, Appl. Phys. Lett. 101, (2012) 052101.

20. Lermusiaux, L.; Mazel, A.; Carretero-Genevrier, A.; Sanchez, C.; Drisko, G. L.; Metal-Induced Crystallization in Metal Oxides, Acc. Chem. Res. (2022) 55, 171−185.

21. Farmer, S.; Predicting the Percentage: Relating the Refractive Index to Effective Medium Theory in Combination Dielectric Films, https://ir.library.oregonstate.edu/concern/undergraduate_thesis_or_projects/vq27zx28k, Undergraduate thesis Oregon State University, 2023.
22. Lafuente, B.; Downs, R. T.; Yang, H.; Stone, N.; Armbruster, T.; Danisi, R. M. eds The Power of Databases: The RRUFF project, Berlin, Germany, W.; De Gruyter, 2015, 1-30.
23. Haggerty, J. E. S.; Schelhas, L. T.; Kitchaev, D. A.; Mangum, J. S.; Garten, L. M.; Sun, W.; Stone, K. H.; Perkins, J. D.; Toney, M. F.; Ceder, G.; Ginley, D. S.; Gorman, B. P.; Tate, J. High-Fraction Brookite Films from Amorphous Precursors, Sci. Rep. 2017, 7, 15232.
24. NIST-JANAF Thermochemical Tables, NIST Standard Reference Database Number 13, DOI: 10.18434/T42S31.
25. NIST Chemistry WebBook, NIST Standard Reference Database Number 69, DOI: 10.18434/T4D303 (Last update: 2023).
26. Mosquera, A. A.; Albella, J. M.; Navarro, V.; D. Bhattacharyya, D.; Endrino, J. L. Effect of Silver on the Phase Transition and Wettability of Titanium Oxide Films, Sci. Rep. 2016, 6, 32171.

Graphical Abstract for:

Role of Sn in the Amorphous-to-Crystalline Transition of TiO_2 Thin Films

Pritha Biswas, Tamara D. Koledin, Skylar N. Farmer, Melissa K. Santala, and Janet Tate

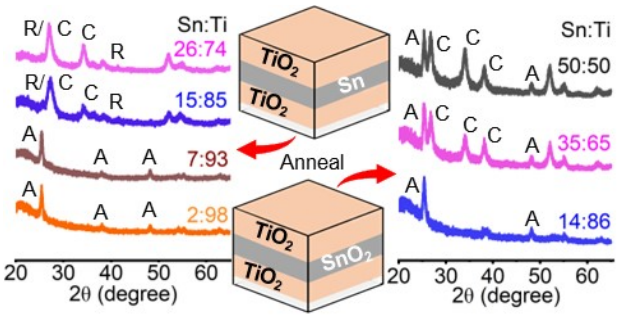

Brief Synopsis (< 60 words)

Amorphous TiO_2 precursor films prepared to yield the *anatase* polymorph upon annealing in air crystallize into the *rutile* polymorph when metal tin is incorporated at sufficient concentration. It is proposed that metal tin acts as an oxygen scavenger, producing an oxygen-deficient environment that favors rutile TiO_2 formation. When tin is incorporated as an oxide in the precursor, no rutile forms.